Corrosion Behavior of NdFeB Magnets in Different Aqueous Solutions

Ana-Maria Popescu, [a] *Jose M. Calderon-Moreno,*[a] *Kazimir Yanushkevish,*[b]
Alexei Aplevich,[b] *Olga Demidenko,* [b] *Elena Ionela Neacsu*[a] *and Virgil Constantin* [*,a]

*a"Ilie Murgulescu" Institute of Physical Chemistry of the Romanian Academy,
Splaiul Independentei 202, Bucharest 060021, Romania*

*bSSPA "Scientific-Practical Materials Research Centre of NAS of Belarus",
19 P. Brovki str., Minsk 220072, Belarus*

Sintered NdFeB magnets possess excellent magnetic properties, but behave passively in alkaline and saline media and are susceptible to corrosion in acidic environments. The corrosion behavior of NdFeB magnets in industrial environments: potassium hydroxide (KOH), perchloric acid ($HClO_4$) and sodium chloride (NaCl), was investigated by immersion and electrochemical tests. The immersion test concluded that the most corrosive electrolyte of the three studied was $HClO_4$. Electrochemical tests showed that the NdFeB sample without magnetic order had better corrosion resistance. Metallographic microscopy and scanning electron microscopy support the obtained corrosion data. X-ray photoelectron spectroscopy indicates that the main elements on the surface of the analyzed sample (Nd, Fe, B) are in the oxidized state after corrosion.

Keywords: NdFeB magnets, corrosion, X-ray diffraction, scanning electron microscopy, energy dispersive X-ray analysis, X-ray photoelectron spectroscopy

Introduction

Neodymium-based permanent magnets are the most recent class of magnetic materials introduced to the market, since 1982. Sintered NdFeB permanent magnets possess excellent magnetic characteristics. $Nd_2Fe_{14}B$ alloy, with high magnetic crystallographic anisotropy, was first obtained in 1979. In 1984, Sagawa *et al.*[1] have shown that, in the ternary system Fe-Nd-B, the approximate composition $Nd_2Fe_{14}B$ is a promising material for permanent magnets in terms of its crystal structure and magnetic properties. The alloys used for the production of permanent magnets, as a rule, differ from the stoichiometric composition of $Nd_2Fe_{14}B$ towards a slightly higher content of neodymium and boron. The increased content of neodymium and boron in the alloy requires suppression of the formation of primary gamma-Fe crystals. During the heat treatment of NdFeB alloys, the formation of the $Nd_2Fe_{14}B$ phase is promoted by heating the alloy above its Curie temperature and holding it at a temperature below the peritectic temperature. At temperatures below the peritectic temperature, $Nd_2Fe_{14}B$ is in equilibrium with a liquid phase enriched in neodymium and boron. This liquid phase is formed by the partial melting of the alloy at temperatures below the peritectic temperature and plays a crucial role in the formation of the $Nd_2Fe_{14}B$ phase by promoting the diffusion of neodymium and boron into the $Nd_2Fe_{14}B$ grains, while avoiding excessive melting or recrystallization that can lead to the formation of gamma-Fe crystals. NdFeB magnets are composed of a complex microstructure consisting of three phases: $Nd_2Fe_{14}B$, Nd-rich phase and eutectic. The $Nd_2Fe_{14}B$ phase is the main component and is responsible for the high magnetic energy product of the magnet. $Nd_2Fe_{14}B$ is a hard magnetic phase with a tetragonal crystal structure. The Nd-rich phase is a soft magnetic phase with body-centered cubic crystal structure. This phase helps to reduce magnetic domain wall energy and increase the coercivity of the magnet. The eutectic phase is a combination of the $Nd_2Fe_{14}B$ and Nd-rich phases, formed during the solidification of the alloy. This phase provides a means of connectivity between the $Nd_2Fe_{14}B$ grains, which helps to increase the mechanical strength of the magnet. Boron-rich phase $NdFe_4B_4$ can be formed at the grain boundaries if excess boron is added during

the manufacturing process to promote the formation of the $Nd_2Fe_{14}B$ phase, but it is not one of the major phases in the microstructure of these magnets, as this phase can reduce the magnet's coercivity, increase its magnetization reversal energy, and lower its thermal stability. Due to the high magnetism, $Nd_2Fe_{14}B$ magnets are used in electrical devices, electromechanical electronics, and more recently even in dental prosthetics.[2]

With the expansion of the fields of application of NdFeB magnets, and the fact that they can be recycled, the requirements for their corrosion resistance have increased, especially when they are used in generators and electric motors. Several researchers[3-7] have used different techniques to evaluate corrosion protection in several electrolytes for the as-received NdFeB magnets or with different protective films. Corrosion depends on the multiphase microstructure of NdFeB magnets.[8-10] This microstructure ensures very good magnetic properties but also low corrosion resistance, being susceptible to various forms of corrosion.[11-13] The presence of Nb-rich or unbound neodymium in ternary eutectic alloys has a negative effect on corrosion properties.

Electrochemical corrosion behavior of NdFeB magnets in different acids (HNO_3, HCl, H_2SO_4, H_3PO_4, $H_2C_2O_4$)[14] indicates that in strong acid solutions with similar hydrogen ion concentration, the corrosion current increases in the order of $HCl > H_2SO_4 > HNO_3$, while NdFeB are passivated in H_3PO_4 and $H_2C_2O_4$. Ni *et al.*[15] followed the behavior of NdFeB magnets in HNO_3-HF mixture solutions using open circuit potential and polarization measurements and impedance spectroscopy. The results showed that HF addition increased the open circuit potential, corrosion potential, and film/inductive/charge transfer resistance, but decreased the magnet corrosion current density. The effects of HF on corrosion performance were closely related to the formation of NdF_3 corrosion products on the surface of the magnet, which in turn depended on its content.

NdFeB magnets have been observed to have a passive behavior in acid ($H_2C_2O_4$) and hydroxide (NaOH) solutions.[16] The electrochemical polarization behavior of a commercial permanent magnet in the magnetized and demagnetized state, with different surface preparation conditions, was evaluated in 0.1 M NaH_2PO_4 solution containing 0-0.017 M of chloride.[17] Bare samples showed passivity in chloride free phosphate solution, while chloride additions caused pitting of the magnets. The corrosion behavior of three commercial sintered NdFeB magnets exposed to environments containing water as vapor, pressurized vapor, and liquid was investigated to understand their overall corrosion performance under a range of conditions. Magnet surface finish had an effect on corrosion

initiation under mild heat-moisture exposure. Immersion in liquid water resulted in a corrosion topography in which the Nd-rich grain-boundary phase did not selectively corrode as in the other accelerated corrosion tests, but was kept intact while the matrix phase corroded.[18] A comparative study of the corrosion behavior of NdFeB magnets in hydroxide, chloride and acid solutions (NaOH, NaCl, HNO_3, $H_2C_2O_4$) was investigated by immersion and electrochemical tests, and HNO_3 was found to be the most strongly corrosive electrolyte.[19] Electrochemical tests results were consistent with the immersion tests and showed passivation of the magnets in NaOH and $H_2C_2O_4$ solutions. NdFeB-based magnets with Dy were investigated in NaCl solution and spontaneous passivation and pitting corrosion were observed.[9]

At the same time, Jilin *et al.*[20] explored the corrosion behavior of conventional NdFeB magnets in different acid solutions (HNO_3, H_2SO_4, and HCl) and found the increase of electrochemical corrosion rate as $HNO_3 < HCl < H_2SO_4$. Recent corrosion studies in 0.1 M NaCl[21] on NdFeB permanent magnets show pitting resistance corrosion. Immersion tests and magnetic property measurements were used to study the long-term effects of electrochemical corrosion in 3.5 wt.% NaCl on the magnetic properties of the NdFeB magnets and analyzing the measurement results, about 90% of the remanence (B_r) loss was attributed to the phase loss of the matrix, while the remaining 10% was attributed to the deterioration of the magnet surface structure during electrochemical corrosion.[22] The work of Shi *et al.*[23] demonstrated that Al/Cr films have great potential to be used to provide effective corrosion and mechanical protection for Nd-Fe-B magnets.

The aim of this article is to investigate the corrosion behavior of sintered NdFeB magnets in different electrolyte solutions (0.5 M KOH, 0.5 M $KClO_4$, and 3 wt.% NaCl) by immersion and electrochemical techniques. The structure and microstructure of the NdFeB magnets are evaluated by X-ray diffraction (XRD), scanning electron microscopy (SEM), energy dispersive X-ray (EDS) and X-ray photoelectron spectroscopies (XPS).

Experimental

Obtaining Nd-Fe-B samples

NdFeB magnets are commonly obtained by sintering from rare earth powders and cooled by an intense magnetic field. The composition must be richer in Nd than the stoichiometric composition of $Nd_2Fe_{14}B$ to compensate for the preferential oxidation of Nd and to retain small amounts of Nd in the Nd-rich phase of the grains in the magnet matrix.

2 of 12

J. Braz. Chem. Soc. **2024**, *35*, 1, e-20230089

The NdFeB samples used in these experiments were provided by Magnequench (Magnequench Technology Center, SG, Singapore). The chemical composition was: Fe: 67.9%, Nd: 26.3%, B: 1.00%, and other elements in very small amounts (Al, Si, Co, Cu, Nb, Dy).

All these alloys are magnetic because they contain an unpaired electron. To obtain samples of $Nd_2Fe_{14}B$ without magnetic ordering, we heated them to a temperature above the T_C (Curie temperature, about 900 K) and quenched them.

In this study, we used two kinds of samples: NFB-M (normal magnetic) and NFB-NM (without magnetic ordering).

Characterization of the structure/microstructure

The crystal structure of the as-deposited thin films was characterized using an X-ray diffractometer DRON-2 (Bourevestnik, Inc., St. Peterburg, Russia) with Cu Kα-radiation in the $20° \leq 2\theta \leq 90°$ angle range. X-ray patterns are received by automatic recording with a scan step of 0.03° and exposure of 2-3 s *per* step.

Micrographic images at ×100-×800 magnifications were obtained with a metallurgical microscope MM (New York Microscope Company, Hicksville, NY, USA) with camera acquisition.

The morphology of the obtained thin films was analyzed by SEM using a microscope Philips XL-30-SEM (SEM Tech. Solutions, Inc., North Billerica, MA, USA) equipped with EDS. The accuracy of the measurements for the equipment used was rated as ± 0.1 wt.%.

Surface analysis of the obtained thin films by XPS was carried out on PHI Quantera SXM equipment, (Physical Electronics, ULVAC-PHI, Chanhassen, MN, USA) with a base pressure in the analysis chamber of 10^{-9} Torr. The X-ray source was Al Kα radiation (1486.6 eV, monochromatized) and the overall energy resolution is estimated at 0.65 eV by the full width at half maximum (FWHM) of the Au4f7/2 line. In order to take into account the charging effect on the measured binding energies (BE) the spectra were calibrated using the C1s line (BE = 284.8 eV, C–C $(CH)_n$ bonds) of the hydrocarbons adsorbed on the sample surface. The deconvolution peaks were identified by reference to an XPS database.[24] We must emphasize that the errors in our quantitative analysis (relative concentrations) were estimated in the range of ± 10%, while the accuracy for BE assignments was ± 0.2 eV.

Corrosion behavior

The weight loss (Δm) measurements have been identified to be a good method for long-term corrosion evaluation of metals in immersion tests. The measurements were done in aerated room temperature solutions of different electrolytes: 0.5 M KOH, 0.5 M $HClO_4$ and 3 wt.% NaCl; all the solutions were prepared using commercially available P.A. reagents from Sigma-Aldrich (Sigma Aldrich Inc., Mo, USA) and deionized water (RiOs-DI® Water Purification System Merck KGaA, Darmstadt, Germany). Mass losses (Δm) were obtained by extrapolating mass loss measurements after each cleaning cycle, according to the ASTM G1-03 standard.[25] Metal mass loss (MML) was evaluated according to the formula: MML = $\Delta m \times K/d \times S_{exp}$, where $K = 8.76 \times 10^4$ represents coefficient that takes into account the measurement's translation of units, $S_{exp} = 6.638$ cm^2 represents surface area of the material exposed, $d = 7.6$ g cm^{-3} represents the density of NdFeB. The corrosion rate (C_R) of NdFeB samples was evaluated by considering the mass loss (Δm) in g, the surface of the sample (S) in cm^2, and the immersion time (t) in h, using the following formula: $C_R = \Delta m/S \times t$.

Electrochemical measurements of two NdFeB specimens (M4 and NM) were made utilizing the potentiodynamic polarisation technique and using a potentiostat/gavanostat model PARSTAT 2273 (Princeton Applied Research, Oak Ridge, TN, USA), with a "Power Corr" Software. For the electrochemical tests we used open circuit potential (OCP), linear polarization (LPR) and Tafel polarization measurements. These tests were performed in a 3 wt.% NaCl aerated aqueous solution under ambient conditions, (25 ± 2) °C and without stirring. All electrochemical tests were performed using a 100 cm^3 thermostatic glass cell with a standard three-electrode system, with the steel samples as the working electrode (WE), the Ag/AgCl reference electrode (saturated with 0.3 M KCl), and a platinum plate with area of 1 cm^2 as counter electrode, both produced by Radiometer (Radiometer Medical ApS., Copenhagen, Denmark). The cell assembly was placed in a Faraday cage to prevent electrical interference.

Disc specimens of 10 mm diameter and 5 mm thickness were embedded with cold resin setter in order to obtain an area of 1 cm^2, after that all electrical contacts were adequately established, leaving only one face exposed to the electrolyte for the electrochemical test. Prior to corrosion tests, the specimens were ground up to 1200 grit emery paper and then cleaned with distilled water and reagent alcohol (Sigma-Aldrich).

To start the experiments, the sample was introduced into the cell and allowed to reach equilibrium, which typically took about 20 min. The OCP experiment was done for 3600 s and finally the E_{OCP} (open circuit potential which is the corrosion potential of the working electrode which was measured relative to a reference electrode since no potential

J. Braz. Chem. Soc. **2024**, *35*, 1, e-20230089

3 of 12

or current is being applied to the cell) was obtained. The linear polarization curves at ± 20 mV were collected starting from the OCP after reaching a constant value (up to 30 min) and from them the polarization resistance (R_p) was calculated.[26] Tafel polarization experiments were performed with a constant scan rate of 0.166 mV s^{-1}, while the potential was shifted within ± 250 mV from the E_{OCP}.[26] When plotting the polarization curves, we take into account that prolonged anodic polarization might give rise to changes at the surface roughness which would imply parallel translation of the Tafel slopes. This effect was eliminated by first plotting the cathodic branches and then the anodic ones. From the Tafel plots the corrosion potential (E_{corr}), the corrosion current density (i_{corr}) and corrosion rate (C_R) were calculated. The corrosion current density i_{corr} was determined either by extrapolating the cathodic and anodic Tafel lines to E_{corr} or according to the Stern-Geary equation.[27]

For the immersion corrosion test, we used 3 normal magnetic samples noted NFB-M1, NFB-M2, and NFB-M3, while for the electrochemical corrosion test 2 samples (without magnetic ordering) NFB-NM1 and (normal magnetic) NFB-M4 were used.

Results and Discussion

Initial characterization of the NdFeB

Figure 1 shows the XRD spectrum for the studied samples. XRD analysis showed that their crystal structure is almost identical, with a sharp peak at 40-50°. This peak corresponds to the tetragonal structure of the composition $Nd_2Fe_{14}B$ (space group: P42/mnm) with 68 atoms in the initial cell.[28,29] It is observed that the diffraction peaks of the $Nd_2Fe_{14}B$ phase such as (204), (224), and (319) are more intense, indicating a certain (00l) texture and also an unexpressed *c*-axis crystallographic alignment. Such a crystal cell provides uniaxial magnetic anisotropy for the $Nd_2Fe_{14}B$ compound. All peaks correspond to the tetragonal structure Figure S1 (Supplementary Information (SI) section). The iron atoms occupy six different non-equivalent positions and the neodymium atoms occupy two positions in the unit cell. The unit cell parameters of $Nd_2Fe_{14}B$ are c = 1.219 nm and a = 0.880 nm.[29] Moreover, in this sample, establishing the existence of the α-Fe phase is very difficult taking into consideration that the (006) peak of the $Nd_2Fe_{14}B$ phase is very close, about 0.02°, to the (110) peak of the α-Fe phase. From the X-ray pattern, the average crystallite size was calculated using the Debye-Scherrer equation:[30,31] $d_{cryst} = 0.9 \times \lambda / B \times \cos \omega$ where d is the grain size, λ is the X-ray wavelength (λ = 0.1542 nm); B is the full width at
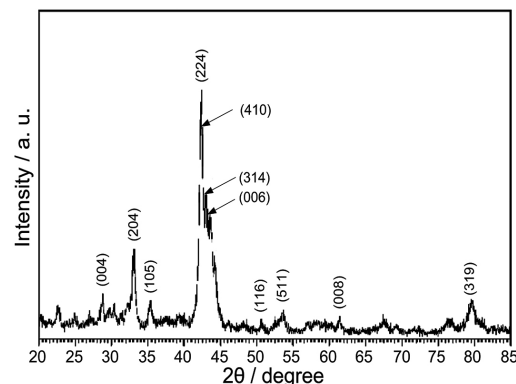
Figure 1. XRD spectra for as-received $Nd_2Fe_{14}B$.

half maximum (FWHM) and (ω) is half the diffraction angle of crystal orientation peak (in radians).

The calculated grain size for the initial NdFeB block is d_{cryst} ca. 13.7 nm. After magnetization, this parameter is equal to d_{cryst} ca. 16.4 nm. This change can be caused by the formation of magnetic centers.

For SEM and XPS, we could perform measurements only on the NFB-NM in order not to damaged the equipment.

The SEM-EDS analysis of the polished NFB-NM sample is presented in Figure 2. The magnets had a dark grey appearance. The morphology of the sample shown in Figure 2a presents a uniform, homogeneous deposit with a mini globular structure at low magnifications (×100-×250), while at high magnifications (×2000) it is observed that it presents some scratches (which can be from sample polishing).

Following the EDS spectrum (Figure 2b), only peaks corresponding to Fe, Nd, and O are observed. Boron does not appear on the EDS spectrum. The EDS spectrum demonstrated the good compositional homogeneity of the studied sample: the chemical composition of the studied magnet is almost the same in different zones, indicating a Fe-rich alloy (68%) with Nd (27%).

These elemental analysis results for the NdFeB magnet are similar to those obtained formerly by other authors.[32]

XPS analysis was used to determine the chemical states of the elements present on the surface of the samples and, after quantitative analysis, to find the relative element and chemical state concentration. It is pertinent to note here that all calculations were performed assuming that the sample were homogeneous within the XPS detected volume. The following values were calculated for the cation relative concentration in NdFeB sample surface before corrosion: 2.05 atom% Nd, 91.81 atom% Fe and 6.14 atom% B.

The surveys XPS spectrum (Figure 3) and high-resolution photoelectron spectra (Figures 4a-4e) of the most prominent XPS transitions (Nd 3d, Nd 4d, Fe 2p, B 1s, and
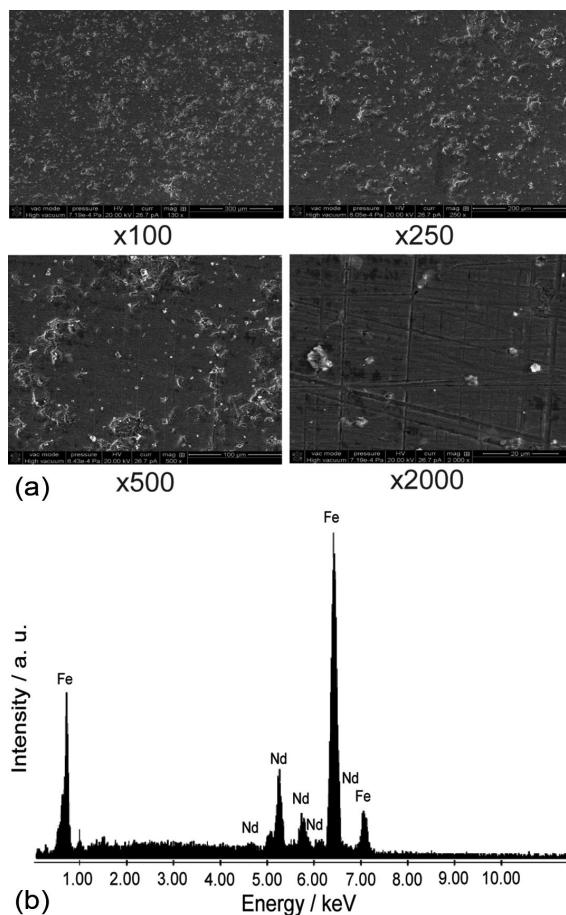
Figure 2. SEM images (a) and EDS spectrum (b) for the initial NFB-NM sample.

O 1s) were recorded for samples before and after corrosion as received and after sputtering (2 min). From the calculated results, substantial amounts of C were detected on the surface, which can be attributed to the fact that the surface of the samples was contaminated with unavoidable carbon from CO_2 and hydrocarbon adsorbed on the outermost layer from the ambient atmosphere. On the surface of the analyzed sample of NdFeB before corrosion, the main elements (Nd, Fe, B) are found to be in an oxidation state.
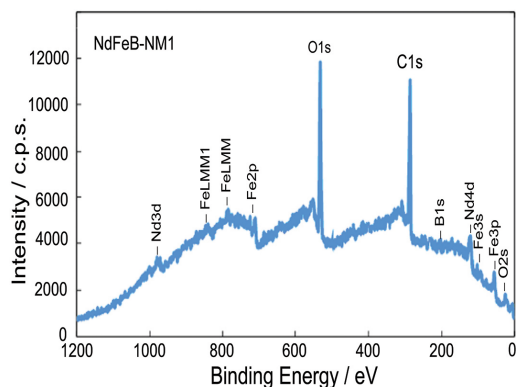
Figure 3. Survey XPS spectrum for the initial NFB-NM sample.

Figure 4 presents the high-resolution spectra of the elements founded in the survey spectrum. Figure 4a shows the deconvoluted peaks for Nd3d where the very clear peak for $Nd(3d_{5/2})$ and the almost overlapping peak of $Nd(3d_{3/2})$ with O KLL are observed. That is why we used Nd4d instead (Figure 4b). We should note that the Nd4d peak is positioned around -120 eV, which is in good agreement with the oxidation state of Nd^{3+}.[33-36] Regarding the deconvoluted spectrum of Fe (Figure 4c) we observe the existence of two shoulders corresponding to $Fe_{(metal)}$ and Fe_2O_3. As for B (Figure 4d), the deconvoluted spectrum shows that boron is oxidized: the peak at ca. -191 eV corresponds to B_2O_3 or a borate form.[36,37] The deconvoluted spectrum of oxygen (Figure 4e) showing two peaks could suggest that not only oxides but also hydroxides were formed. But because the largest peak is at 530 eV, this means that mainly metal oxides formed.[33,34] SEM and XPS measurements could not be performed for the normal magnetic (NFB-M) samples due to the limitation of the working equipment (due to the strong magnetic field).

Corrosion behavior of Nd-Fe-B

Immersion corrosion test

The NdFeB magnets were immersed in the following solutions: 0.5 M KOH, 0.5 M $HClO_4$, and 3 wt.% NaCl (which in actually ca. 0.5 M NaCl), at room temperature (ca. 22 °C) for about half a year in which 12 measurements were performed for each sample and the final results were the average value of the 12 measurements. After the immersion test, the corrosion products were removed according to ASTM G1-03 (ISO 8407:199)[25] and, according to the analysis protocol, the samples were dried and weighed. The time evolution of the mass loss (mg cm^{-2}) and the calculated corrosion rate (mm $year^{-1}$) are presented in Figure 5.

Following the graphs in Figure 5a, it can be seen that after ca. 72 h of immersion the metal loss is somewhat constant for immersion in NaCl and KOH, but has slight increases in $HClO_4$.

The same evolution has the corrosion rate of NdFeB in the three solutions (Figure 5b). It should be stated that the significant mass loss occurs in the first 24 h after immersing the samples, then after ca. 100 h there is a sudden decrease in the mass loss, respectively the corrosion rate, which suggests a passivation of the magnetic material. The corrosion resistance is relatively good, which can be seen from the calculation of the penetration index, which falls into stability class 2-3, being very stable in the studied solutions. According to the comparison of metal mass losses and the calculation of the average C_R for the three immersion
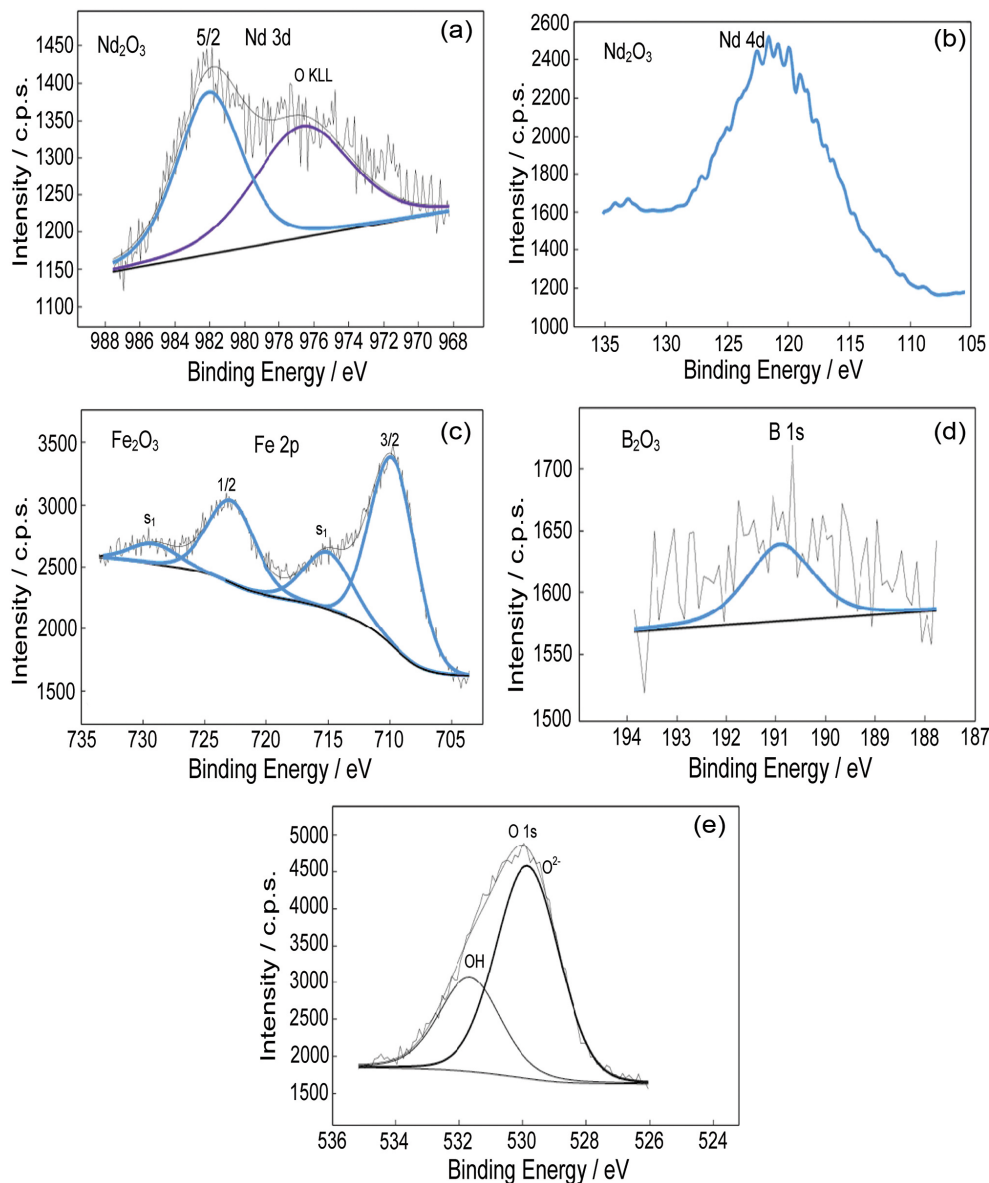
J. Braz. Chem. Soc. **2024**, *35*, 1, e-20230089

5 of 12

Figure 4. XPS high resolution spectra for the initial NFB-NM sample: (a) Nd 3d$_{5/2}$, (b) Nd 4d, (c) Fe 2p, (d) B 1s and (e) O 1s high resolution spectra.
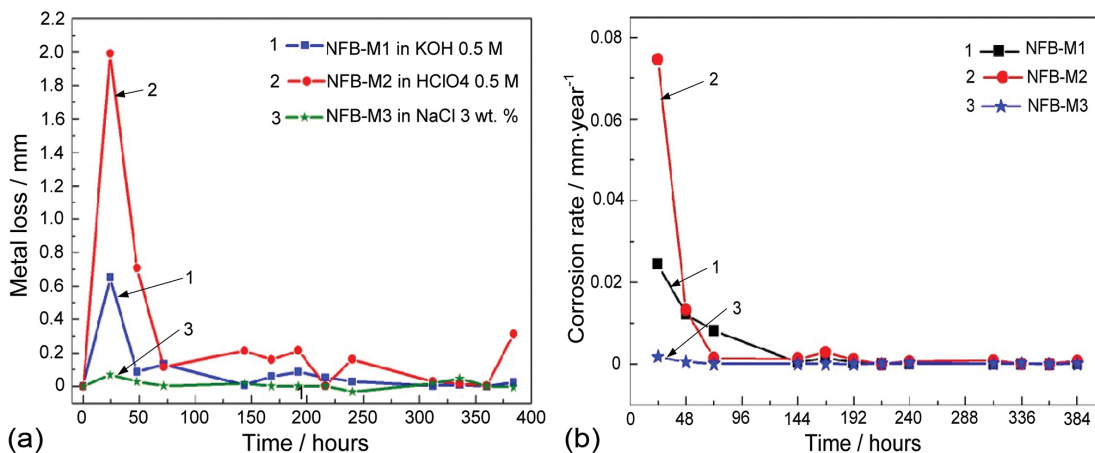

Figure 5. (a) Mass loss *vs*. time; (b) corrosion rate *vs*. time for NdFeB immersed in different solutions.

6 of 12

J. Braz. Chem. Soc. **2024**, 35, 1, e-20230089

solutions (C_R(average) in KOH = 0.0038075 mm year^{-1}; C_R(average) in HClO$_4$ = 0.0079575 mm year^{-1}; C_R (average) in NaCl = 0.002357 mm year^{-1}), we can conclude that the attack properties of the three electrolyte solutions on magnetized NdFeB samples increases in the sequence NaCl < KOH < HClO$_4$. Regarding the corrosion of sample M2 in HClO$_4$, in addition to the strong corrosive effect of perchloric acid due to the presence of both oxygen and chlorine, the initial structure of this sample, which showed cracks that may be functional as seeds of corrosion, should be considered.

To reveal the exact corrosion mechanism, the evolution of the sample surfaces was followed by microscopy before and after corrosion coupled with photo images of the samples after corrosion, finding a good agreement with the obtained immersion corrosion data.

Photographic images (Figure 6) show the magnets after being corroded in different solutions for 400 h. The evolution of the appearance of the corroded samples can be clearly observed on these photos. A layer of granular dark grit deposit is found on all samples; in the case of sample M2, the corrosion process is so strong that it even caused part of the sample to break; also, there is a difference between corrosion on polished and unpolished samples in the sense that on the unpolished face (so in the conditions in which these magnets will be used on an industrial scale) the corrosion process is more pronounced. This is due to the surface roughness of the sample. Photographic images of the magnetized NFB samples after corrosion confirm the mass loss test results, proving once again that the sample immersed in perchloric acid underwent the strongest corrosion process.
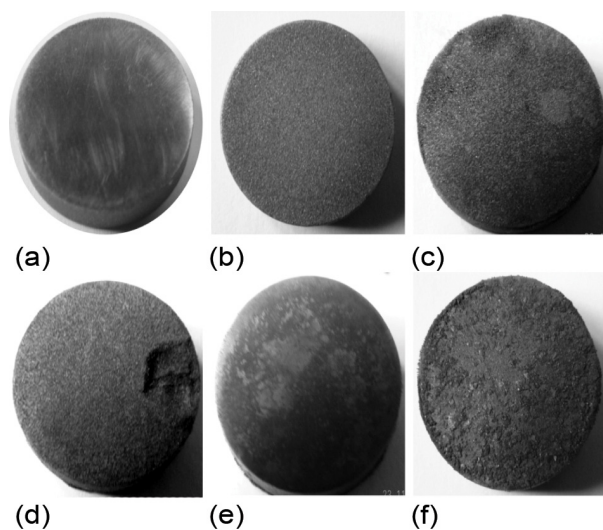
Figure 6. Photographic images of NFB samples: (a) initial sample; (b-f) after corrosion for 400 h; (b) sample M1 in KOH electrolyte; (c-d) sample M2 in HClO$_4$ (c) polished face; (d) unpolished face; (e-f) sample M3 in NaCl (e) polished face; (f) unpolished.

The same evolution is evidenced by the MM images (magnification ×100-×400) of the samples before and after corrosion, presented in Figures 7-9.

Regarding the KOH solution, it showed a medium attack on the NFB-M1 sample considering the lower weight loss, and the micrographic images indicate a slight modification of the surface (Figure 7b), in agreement with those previously obtained in NaOH solution.[19]
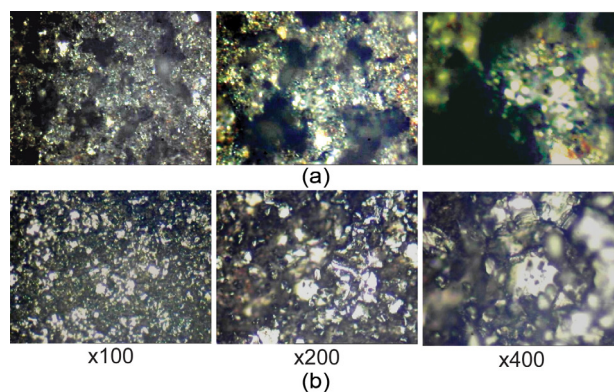
Figure 7. Micrograph of sample NFB-M1, at ×100 and ×400 magnification: initial stage, (b) long term corrosion in 0.5 M KOH solution.

The optical micrographs for the NFB-M2 sample, in initial stage, at different magnifications is presented in Figure 8a. The corroded NFB-M2 in the KClO$_4$ solution (Figure 8b) indicate a major change of the surface after corrosion due to the appearance of orange-reddish areas typical of Fe$_2$O$_3$ rust formation and more prominent than other samples. This aggressive behavior of the perchloric acid on the sample was based on the dissolution of Fe and Nd in the upper layer and the released hydrogen led to the embrittlement of the sample, the presumed mechanism is: the Nd-rich phase was corroded rapidly leading to intergranular corrosion.[32]
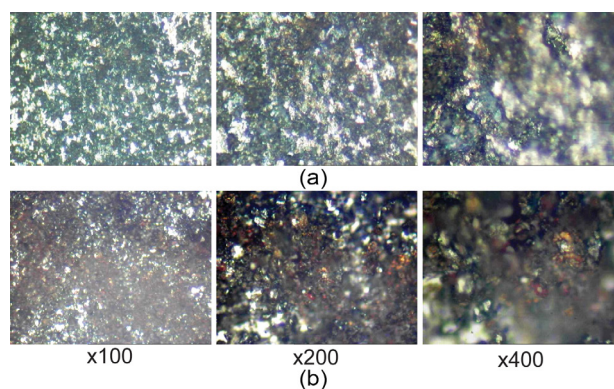
Figure 8. Micrograph of sample NFB-M2: (a) initial stage, (b) long term corrosion in 0.5 M HClO$_4$.

The sample NFB-M3 introduced in the NaCl solution behaved differently, a small weight loss is observed and

J. Braz. Chem. Soc. **2024**, *35*, 1, e-20230089

7 of 12

the micrographs indicate an insignificant surface change (Figure 9b). This result is similar to the data previously obtained by other researchers.[19] It can be said that pits susceptible to pitting corrosion were formed on the surface of the sample: following the balance $Fe \rightarrow Fe^{3+} + 3e^-$ respectively $Nd \rightarrow Nd^{3+} + 3e^-$, i.e., the release of Fe and Nd ions led to the formation of $FeCl_3$ and $NdCl_3$ which penetrated the magnet matrix and led to the formation of pits on the surface.[38,39]
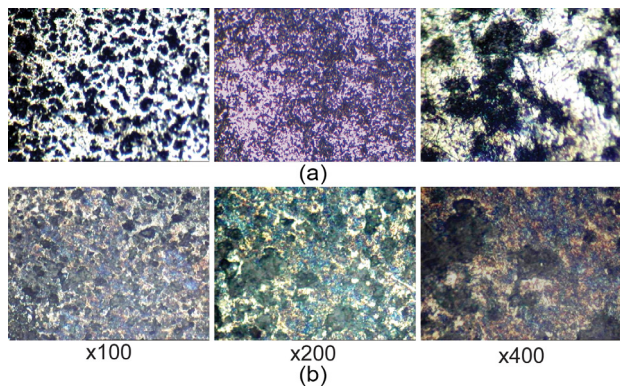
Figure 9. Micrographs of polished NFB-M3: (a) initially, (b) after long term corrosion in 3 wt.% NaCl.

Considering the evolution of the weight loss of the samples in the three electrolytes, the attack sequence can be given: $HClO_4 > KOH > NaCl$.

After corrosion, the XRD study reveals that the peaks corresponding to $Nd_2Fe_{14}B$ (shown in Figure 1) are replaced by broad peaks corresponding to amorphous or slightly crystalline Fe or even Fe_2O_3 and Nd oxide. This suggests that the outer black layer is mainly composed of hematite (Fe_2O_3) and the grayer colored substrate is composed of amorphous Nd oxide particles.

We need to clarify that the external magnetic field for sample demagnetization and corrosion action is not able to introduce significant changes in the bulk crystal structure of the samples. The external magnetic field for demagnetization can only change the domain structure, while corrosion can only change the surface of the sample. So, in these cases, the XRD method is not applicable. Therefore, we have not shown XRD patterns of the demagnetized sample and the sample after corrosion.

In addition, as the photographic images of the sample

immersed in NaCl show an amount of rust deposited on the unpolished face, although the corrosion results showed average corrosion in this environment, it was decided to continue the electrochemical corrosion study in this environment.

Electrochemical corrosion tests

Electrochemical measurements to evaluate the corrosion process were done by OCP, linear polarization and Tafel plots. Figure 10 shows the Tafel plots obtained from the polarization curves of the magnet samples in the 3.5 wt.% NaCl solution. The corresponding calculated corrosion parameters are presented in Table 1.
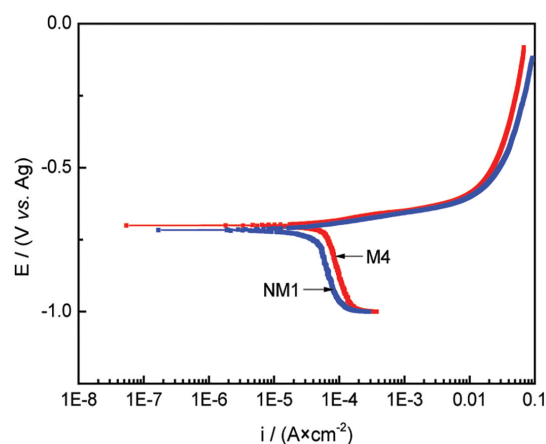
Figure 10. Tafel plots obtained by polarization for samples NFB-NM1 and NFB-M4 in 3.5 wt.% NaCl solution.

The evolution of the data in Table 1 shows that the NFB-M4 and NFB-NM block samples have equal OCP potentials, but the NFB-M4 sample has a three times lower corrosion rate than the NFB-NM sample, which leads to the conclusion that the magnetic ordering has a positive influence on the corrosion resistance of magnets. Data from Table 1 show that E_{corr} values are shifted positively and i_{corr} values decreased from non-magnetized sample to sample with magnetic order.

This hypothesis is also supported by the higher R_p values and the lower i_{corr} value for magnetically ordered NdFeb. Our corrosion results of NdFeB magnets in 3 wt.% NaCl (0.5 M) are in very good agreement with those of Song *et al.*[19]

Table 1. Corrosion kinetic parameters calculated from the polarization curves

Sample	E_{OCP} / V	R_p / Ω	σ	E_{corr} / V	σ	i_{corr} / (A cm^{-2})	σ	C_R / (mm year^{-1})
NFB-NM	−0.747	275.09	0.54	−0.715	0.001	1.717×10^{-7}	1.04×10^{-9}	0.689
NFB-M4	−0.747	318.85	0.38	−0.701	0.001	5.463×10^{-8}	3.51×10^{-10}	0.277

E_{OCP}: open circuit potential; R_p: polarization rate; E_{corr}: corrosion potential; i_{corr}: corrosion current density; C_R: corrosion rate; σ: standard deviation error.
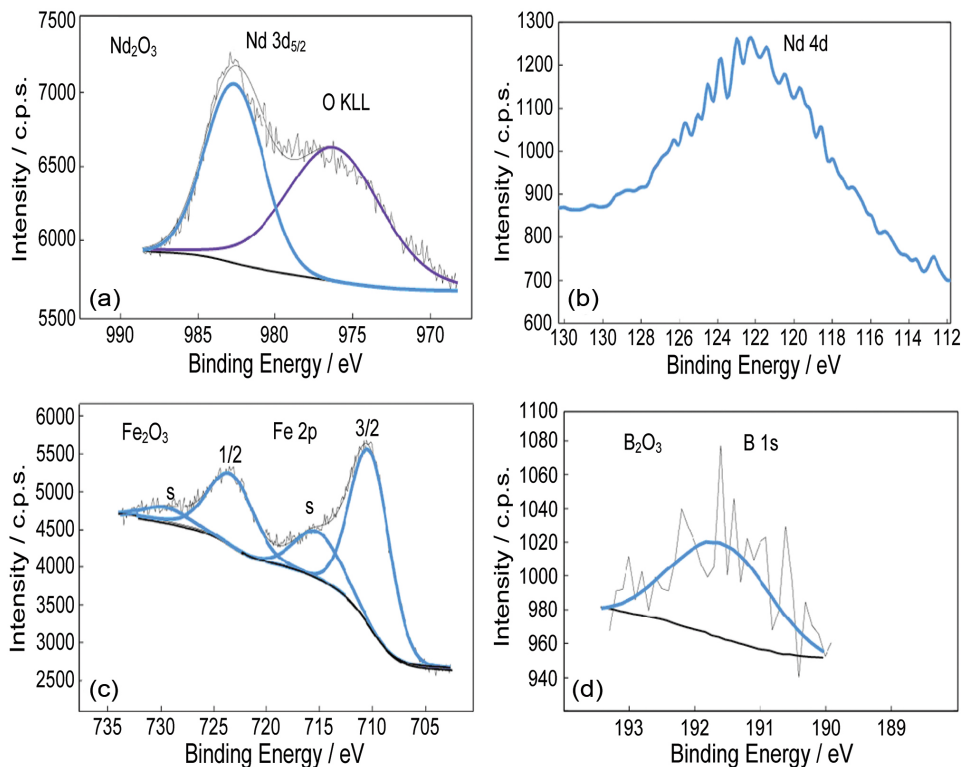
Characterization of corroded NdFeB samples

To determine the products formed as a result of corrosion, measurements of the morphology and surface condition (by SEM and XPS) of the NFB-NM block sample after corrosion were performed. The SEM images presented in Figure 11 show the morphological changes. SEM images indicate the modification of the structure with the appearance of net-like formations, which suggests the existence of an oxide/hydroxide layer on the NdFeB surface.
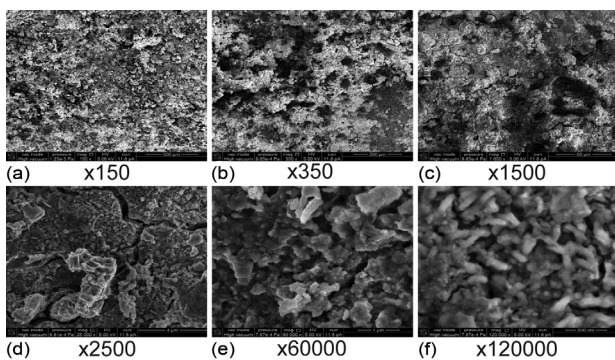

Figure 11. SEM images for the electrochemical corroded NFB-NM sample.

To understand the chemistry of these formations on the surface of the corroded NFB-NM sample, XPS experiments were carried out. The survey spectrum of corroded NdFeB (Figure 12) shows the most prominent XPS transitions (Nd 3d, Nd 4d, Fe 2p, B 1s, and O 1s). C1s appears again, due also to impurities from sample handling.
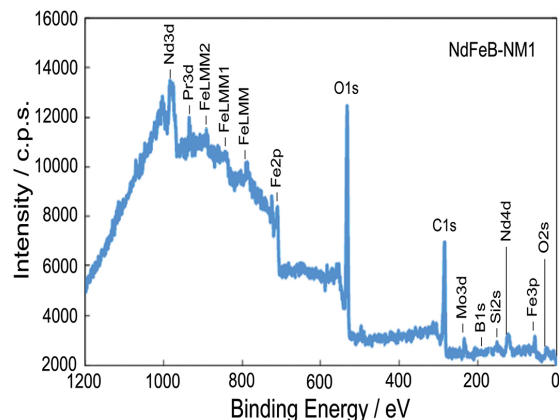
Figure 12. XPS survey spectrum for the corroded NFB-NM sample.

Figure 13 shows the deconvoluted spectra of the corroded NFB-NM. From these spectra it is concluded that all the elements of the alloy after corrosion are present in oxidized form (Nd_2O_3, Fe_2O_3, B_2O_3). The composition of the passive film is estimated to be made of oxides, this composition being maintained, both on the surface (the first 20 nm), after a 2-min cleaning, and on the inside (bulk). The calculated relative concentration of cations

Figure 13. XPS spectra for the electrochemical corroded NFB-NM sample: (a) Nd 3d$_{5/2}$; (b) Nd 4d; (c) Fe2p; (d) B 1s high resolution spectra.

J. Braz. Chem. Soc. **2024**, *35*, 1, e-20230089

9 of 12

found were: 12.79 atom% Nd, 83.50 atom% Fe and 3.71 atom% B. If we compare those results with those for the NdFeB sample before corrosion, we observe an increase in the concentration of Nd and a decrease in Fe and B concentration for the corroded sample, which is in normal magnetic order (NFB-NM) and is correlated with a higher corrosion rate. This increase in Nd concentration leads to a decrease in corrosion resistance, the sample without magnetic order is less corrosion resistant than one with normal magnetic order (NFB-M).

Figure 13a shows the deconvolution spectrum of Nd 3d5/2. The presence of an oxygen phase (O at ca. 975 eV) is observed due to the existence of the corrosion product Nd_2O_3,[34] suggesting the existence of an oxide layer on the NdFeB surface.
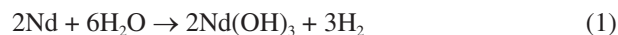
Stable Nd_2O_3 oxide was found that to form at the triple junction at the edge of sintered NdFeB grains upon contact with moisture and, with increasing oxygen, the α-Nd and unstable NdO_x are changed to stable Nd_2O_3.[35] Increasing nitrogen also helps the process of conversion to Nd_2O_3 leading to better corrosion resistance. The fact that we have the Nd4d transition on the spectra (Figure 13b) indicates that the Nd signal is from the bulk of the sample. At the same time, we can consider that the oxidation of the Nd-rich phase of NdFeB can be beneficial and increase the corrosion resistance by decreasing the neodymium-rich marginal layer, so the more neodymium oxide there is, the more corrosion resistant it is. This has already been shown that after several hours oxygen can diffuse deep into the NdFeB matrix and that Nd is mainly responsible for the oxidation.[40]

The BE (eV) values for the main elements from initial/corroded NFB are presented in Table 2, showing that the main modification is on the binding energy of $Nd3d_{5/2}$, confirming the above idea that the oxidation of Nd-rich phase of the NdFeB can be beneficial and increase the corrosion resistance by decreasing the marginal layer rich in neodymium, so the more neodymium oxide there is, the more corrosion-resistant the sample will be.

Table 2. The binding energy (BE) for elements on the surface before and after corrosion process

Sample	BE / eV			
	Nd 3d$_{5/2}$	Nd 4d	Fe 2p$_{3/2}$	B 1s
NFB-NM (initial)	980.0	122.5	710.0	190.9
NFB-NM (corroded)	982.2	122.3	710.6	190.0 (192.0)

Taking into account all these aspects and the literature data[37,41] a corrosion mechanism of these NdFeB alloys in aqueous and aerated environments can be developed as follows:

$$2Nd + 6H_2O \rightarrow 2Nd(OH)_3 + 3H_2 \qquad (1)$$
$$2Nd + 3H_2O \rightarrow Nd_2O_3 + 3H_2 \qquad (2)$$
$$2Nd + O_2 \rightarrow Nd_2O_3 \qquad (3)$$

It was found that the stable Nd_2O_3 oxide is formed at the triple junction at the edge of the sintered NdFeB grains upon contact with humidity or high temperature.[37]

It can be concluded that the same thing happens in the case of an oxygenated atmosphere, so in an aerated solution. This explains the presence of neodymium oxide on the XPS deconvoluted spectra and the existence of the smaller peak corresponding to O, due to the existence of $Nd(OH)_3$.

At the same time, we can consider that the oxidation of the Nd-rich phase of NdFeB can be beneficial and can lead to an increase in corrosion resistance by reducing the marginal layer rich in neodymium, so the more neodymium oxide there is, the more resistant the sample will be to corrosion.

Conclusions

In this article, we have followed the corrosion behavior of NdFeB magnets in different electrolytes through immersion and electrochemical tests. The corrosion test proved that the most corrosive electrolyte was perchloric acid. Also, the electrochemical test in sodium chloride electrolyte showed that the magnetic ordering has a positive influence on the corrosion resistance of the magnets.

This corrosion process was correlated with the microstructure of the magnets. X-ray analysis confirmed the presence of the tetragonal space group structure. Due to the fact that after magnetization the unit cell parameter rises, it may be caused by the formation of magnetic centers. The SEM images of the uncorroded magnets indicate a uniform, homogenous deposit with a mini-globular structure, while following the corrosion process, a modification in structure was observed suggesting the existence of an oxide/hydroxide layer on the NdFeB surface. The XPS study proved the passivation of these magnets during the corrosion process in sodium chloride, due to the oxides formed on the surface of the magnets during corrosion. Oxidation of the Nd-rich phase of NdFeB can be beneficial and is able to increase the corrosion resistance by decreasing the marginal layer rich in neodymium, so the more neodymium oxide there is, the more corrosion-resistant the sample will be.

However, to increase the corrosion resistance of these magnets, the need for coatings with much more resistant materials is estimated.

10 of 12

J. Braz. Chem. Soc. **2024**, *35*, 1, e-20230089

Supplementary Information

Acknowledgments

Author Contributions

Ana-Maria Popescu was responsible for conceptualization, methodology, project administration, investigation of immersion and polarization tests, data curation, writing-original draft/review, validation, supervision, funding acquisition; Jose M. Calderon-Moreno for SEM-EDX investigation, validation and formal analysis; Kazimir Yanushkevish for investigation of XRD, resources, supervision; Alexei Aplevich for investigation of the synthesis and formal analysis; Olga Demidenko for XRD data curation, software, formal analysis investigation and visualization; Elena Ionela Neacsu for XPS investigation, formal analysis and data validation; Virgil Constantin for investigation of electrochemical and micrographic study, software, validation, visualization, writing-review and editing, supervision.

References

1. Sagawa, M.; Fujimura, S.; Togawa, N.; Yamamoto, H.; Matsuura, Y.; *J. Appl. Phys.* **1984**, *55*, 2083. [Crossref]

2. Mastsuura, Y.; *J. Magn. Magn. Mater.* **2006**, *303*, 344. [Crossref]

3. Hosseini, H. R. M.; Dadoo, A.; Dolati, A.; Kianvash, A.; *J. Alloy Compd.* **2006**, *419*, 337. [Crossref]

4. Rada, M.; Gebert, A.; Mazilu, I.; Khlopkov, K.; Gutfleisch, O.; Schultz, L.; Rodewald, W.; *J. Alloy Compd.* **2006**, *415*, 111. [Crossref]

5. Gurappa, I.; *Mater. Chem. Phys.* **2003**, *78*, 719. [Crossref]

6. Tattam, C.; Williams, A. J.; Hay, J. N.; Harris, I. R.; Tedstone, S. F.; Ashraf, M. M.; *J. Magn. Magn. Mater.* **1996**, *152*, L275. [Crossref]

7. Martins, E. A.; Oliveira, M. C. L.; Rossi, J. L.; Costa, I.; de Melo, H. G.; *J. Braz. Chem. Soc.* **2011**, *22*, 264. [Crossref]

8. Schultz, L.; El-Aziz, A. M.; Barkleit, G.; Mummert, K.; *Mater. Sci. Eng.* **1999**, *A267*, 307. [Crossref]

9. El-Moneim, A. A.; *Corros. Sci.* **2004**, *46*, 2517. [Crossref]

10. Costa, I.; Oliveira, M. C. L.; Takiishi, H.; Saiki, M.; Faria, R. N.; *Key Eng. Mater.* **2001**, *189-191*, 340. [Crossref]

11. Dobrzanski, L. A.; Drak, M.; *J. Mater. Process. Technol.* **2004**, *157-158*, 650. [Crossref]

12. Dobrzanski, L. A.; Drak, M.; Trzaska, J.; *J. Mater. Process. Technol.* **2005**, *164-165*, 795. [Crossref]

13. El-Moneim, A. A.; Gebert, A.; Uhleman, M.; Gutfleisch, O.; Schultz, L.; *Corros. Sci.* **2002**, *44*, 1857. [Crossref]

14. Jingwu, Z.; Liqiang, J.; Qiaoling, C.; *J. Rare Earths* **2006**, *24*, 218. [Crossref]

15. Ni, J.; Cui, X.; Liu, X.; Cui, H.; Xue, Z. C.; Jia, Z.; Wang, C.; Ma, J.; Gong, S.; *Mater. Chem. Phys.* **2015**, *162*, 518. [Crossref]

16. Zhang, H.; Song, Z. L.; Mao, S. D.; Yang, H. X.; *Mater. Corros.* **2011**, *62*, 346. [Crossref]

17. Chitrada, K.; Raja, K. S.; Pesic, B.; Charit, I.; *Electrochim. Acta* **2014**, *123*, 23. [Crossref]

18. Isotahdon, E.; Huttunen-Saarivirta, E.; Heinonen, S.; Kuokkala, V. T.; Paju, M.; *J. Alloys Compd.* **2015**, *626*, 349. [Crossref]

19. Song, Y. W.; Zhang, H.; Yang, H. X.; Song, Z. L.; *Mater. Corros.* **2008**, *59*, 794. [Crossref]

20. Jilin, X.; Zhengxian, H.; Junming, L.; Zhenchen, Z.; *Rare Met. Mater. Eng.* **2015**, *44*, 786. [Crossref]

21. Skotnicova, K.; Kolchugina, N. B.; Cegan, T.; Prokofev, P. A.; Lasek, S.; Jurica, J.; Dormidontov, N. A.; Bakulina, A. S.; Rusinov, D. A.; *J. Phys.: Conf. Ser.* **2021**, *1758*, 012038. [Crossref]

22. Zhang, K.; Fan, E.; He, J.; Li, X.; Huang, Y.; *J. Magn. Magn. Mater.* **2021**, *538*, 168309. [Crossref]

23. Shi, Z.; Zeng, H.; Zhang, Z.; Zhang, X.; Curkovic, L.; Mandic, V.; Fu, S.; Wang, W.; Liu, J.; Zhao, L.; Zhang, X.; *J. Magn. Magn. Mater.* **2023**, *565*, 170222. [Crossref]

24. Moulder, J. F.; Stickle, W. F.; Sobol, P. E.; Bomben, K. D.; *Handbook of X-ray Photoelectron Spectroscopy*; ULVAC-PHI Inc: Chigasaki, JP, 1995.

25. ASTM G1-03: *Standard Practice for Preparing, Cleaning, and Evaluating Corrosion Test Specimens*; West Conshohocken, 2017.

26. Yang, L.; Li, J.; Zheng, Y.; Jiang, W.; Zhang, M.; *J. Alloy Compd.* **2009**, *467*, 562. [Crossref]

27. Stern, M.; Geary, A. L.; *J. Electrochem. Soc.* **1957**, *104*, 56. [Crossref]

28. *JCPDS-ICDD PCPDFWIN*, v. 2.01; Diffraction pattern file 86-0273; International Center for Diffraction Data, USA, 1998. [Link] accessed in May 2023

29. Herbst, J. F.; Croat, J. J.; Pinkerton, F. E.; *Phys. Rev. B* **1984**, *29*, 4176. [Crossref]

30. Langfort, J. I.; Wilson, A. J. C.; *J. Appl. Cryst.* **1978**, *11*, 102. [Crossref]

31. Scherrer, P.; *Nachr Ges Wiss Gottingen Math-Phys Kl.* **1918**, *1918*, 98. [Link] accessed in May 2023

J. Braz. Chem. Soc. **2024**, *35*, 1, e-20230089

11 of 12

32. Isotahdon, E.; Huttunen-Saarivirta, E.; Kuokkala, V. T.; Paju, M.; *Mater. Chem. Phys.* **2012**, *135*, 762. [Crossref]

33. Salih, K. A. M.; Hamza, M. F.;Mira, H.; Wei, Y.; Gao, F.; Atta, A. M.; Fujita, T.; Guibal, E.; *Molecules* **2021**, *26*, 1049. [Crossref]

34. Uwamino, Y.; Ishizuka, T.; Yamatera, H.; *J. Electron. Spectrosc. Relat. Phenom*. **1984**, *34*, 67. [Crossref]

35. Ong, C. W.; Huang, H.; Zheng, B.; Kwok, R.; W. M.; Hut, Y. Y.; Lau, W. M.; *J. Appl. Phys.* **2004**, *95*, 3527. [Crossref]

36. Abd El-Naser, A.; Abdel-Khalek, E. K.; Nabhan, E.; Rayan, D. A.; Gaafar, M. S.; Abd El-Aal, N. S.; *Philos. Mag*. **2021**, *101*, 710. [Crossref]

37. Camp, F. E.; Kim, A. S.; *J. Appl. Phys*. **1991**, *70*, 6348. [Crossref]

38. Googan, C.; *Marine Corrosion and Cathodic Protection*; CRC Press-Taylor & Francis Group: Oxfordshire, UK, 2022. [Crossref]

39. Li, Y.; Evans, H. E.; Harris, I. R.; Jones, I. P.; *Oxid. Met*. **2003**, *59*, 167. [Crossref]

40. Oswald, S.; Fahler, S.; Baunack, S.; *Appl. Surf. Sci*. **2005**, *252*, 218. [Crossref]

41. Jacobson, J.; Kim, A.; *J. Appl. Phys.* **1987**, *61*, 3763. [Crossref]